IEEE Access
Multidisciplinary ⋮ Rapid Review ⋮ Open Access Journal

Received 24 December 2023, accepted 16 January 2024, date of publication 23 January 2024, date of current version 31 January 2024.

Digital Object Identifier 10.1109/ACCESS.2024.3357726

RESEARCH ARTICLE

Performance Analysis of a High Gain Bidirectional DC-DC Converter Fed Drive for an Electric Vehicle With Battery Charging Capability During Braking

C. P. RAGASUDHA AND S. HEMAMALINI, (Senior Member, IEEE)
School of Electrical Engineering, Vellore Institute of Technology, Chennai, Tamil Nadu 600127, India
Corresponding author: S. Hemamalini (hemamalini.s@vit.ac.in)

ABSTRACT This research presents a novel non-isolated high gain bidirectional DC-DC converter (BDC) and its application in integrating energy storage system with electric vehicle (EV). The proposed converter can provide high voltage gain with the help of two duty cycle operation by employing fewer components in its circuit design. The proposed topology makes use of dual current path inductor structures which reduces their size and eliminates the need for an additional clamping circuit to power the load. Without using voltage multiplier cells (VMC) or hybrid switched-capacitor approaches, the proposed converter can achieve a significant voltage gain. The simulation of the proposed converter-based drive is carried out using MATLAB/Simulink and OPAL-RT software in loop (SIL) system and the performance analysis is done for different driving conditions. The converter powers the motor through the battery during the forward motoring mode. The motor acts as a generator during regenerative braking and the energy is transferred back through the converter to the battery which stores the recovered energy.

INDEX TERMS Bidirectional dc–dc converter, high voltage gain, electric vehicle, regenerative braking, battery charging, OPAL-RT.

I. INTRODUCTION

Governmental bodies and organizations are enforcing stricter limits for fuel consumption and emissions due to the rising rate of oil consumption in the transportation sector, as well as growing concerns over the impact of global warming and the depletion of energy resources. By 2040, it is predicted that the yearly sales of EVs and Hybrid Electric Vehicles (HEVs) would surpass those of petrol and diesel vehicles, with sales of over 48 million [1]. The automobile industry is concentrating on the development of new technologies for the power train, battery, and charging infrastructure in response to the rising demand for vehicles with better fuel efficiency and less impact on the environment. The installation of a high-energy battery pack and regenerative braking aid in extending the driving range and battery life of electric vehicles.

Power electronic converters find its application in drivetrain to modulate the power flow from battery to the propulsion motors and to facilitate regenerative braking in the reverse direction. To increase efficiency and power density, the drivetrain motor and propulsion inverter are made to operate at higher voltage [2]. To raise the battery voltage to the desired level, a boost converter is used. It also enhances the overall performance of the drivetrain by delinking the battery voltage and the inverter dc link voltage [3]. The DC-DC converter must be bidirectional because the forward mode will face transient and overload conditions during which power gets transferred from the battery to load and during the reverse mode, the battery pack is to be charged. Some of the benefits derived by providing a BDC between the

The associate editor coordinating the review of this manuscript and approving it for publication was Liu Hongchen.

battery and the inverter [4], [5] are: a) It reduces the stress on the inverter with an additional DC stage b) It adjusts the inverter supply voltage to increase the motor output, c) The cost and size of the battery can be reduced because of lower cell count requirement and d) The system voltage and battery can be individually designed by the manufacturers. This architecture thus enables versatile system designs for vehicles with various output characteristics. For instance, the battery nominal voltage in the 2010 Toyota Prius is about 200 V, while the DC-DC converter raises the voltage of the dc bus to about 650 V [2].

The most common BDC is the one with an isolated framework [2], [6], [7], [8], [9], [10], [11]. These isolated converters employ the high frequency transformer throughout the operation, increasing its losses and volume. Transformer core saturation [25] is another issue with this kind of converter. Additionally, many isolated converter configurations, such as LLC converters, CLLC converters and dual-active-bridge (DAB) converters, which are the most prevalent kind of isolated BDCs, call for a significant number of active switches [10], [11]. Therefore, non-isolated BDCs are typically preferred when isolation is not mandatory. This is due its simple structure and low component count, which draw the attention of several researchers. They are suitable for some applications, such as the drive train of an electric vehicle, where size and weight are crucial considerations.

To attain high conversion ratios, non-isolated BDCs employ many circuit principles, including SEPIC/Cuk/Zeta, voltage multiplier cells, switching capacitors, and linked inductors. Due to their cascaded construction, SEPIC/Cuk/Zeta converters have a low efficiency and higher voltage stress. BDCs can be designed using voltage multiplier cells; however, this is restricted by the high voltage across switches. BDCs [12], [13], [14] utilize switched capacitors that perform better, have a simpler construction, and require less control complexity. However, for high-gain applications, the circuit becomes progressively complex and is susceptible to losses with the growing number of switches and capacitors.

The system efficiency can be increased with hybrid topologies, but there is insufficient voltage gain and a greater ripple current [15] associated with few of these topologies. However, high conversion factors can be attained using hybrid architectures like SEPIC/quasi-Z source with switched capacitors [16], [17]. Conversion efficiency is nonetheless limited by a high component count and its inability to provide soft switching. Large ripple current at the LV side is a prevalent issue with all high gain non-isolated BDC circuits as it shortens the life and degrade the performance of the battery. Large capacitors can control input ripple current [18], but it is not the preferred option due to the added bulk and cost to the system. Interleaved DC-DC converter is a better option to reduce the input current ripple, but it has a lower voltage gain and more components [19].

Another significant advancement in this regard is the coupled inductor-based bidirectional converter (CIBDC) architecture [20], [21], [22], [23], [24], [25] that aims to achieve a high voltage conversion ratio. Contrary to transformer-based topologies, these coupled inductor-based systems [20] allow energy exchange at several instants during the course of a single time period. By carefully planning the circuit, switch current and voltage stress can be reduced as well. Clamping the coupled inductor's leakage energy and minimizing voltage spikes and stress across switches are major challenges in coupled inductor topologies. By raising the coupled inductance at the low voltage side, the CIBDC proposed in [21] could minimize the current ripple. But it restricts the number of turns of other windings and in turn the voltage transfer ratio of the BDC. The CIBDC suggested in [24] employs two secondary coupled inductor branches to obtain a greater voltage conversion ratio and current sharing features in addition to soft switching. A non-isolated high gain converter for microgrids is suggested in [26], where coupled inductor is substituted by a normal inductor to make the topology appropriate for high voltage conversion application. However, it is unidirectional. The proposed converter is a modified version of the converter in [26] with bidirectional capability for electric vehicle applications.

The proposed high gain bidirectional converter (HGBDC) utilizes only four active power switches which makes its construction simple. High voltage gain is achieved by choosing the appropriate duty cycle and designing proper inductor and capacitor values. Operation of the converter at a lower duty ratio reduces the core saturation problem of the inductor. Furthermore, the input current is divided among the inductors, which reduces their size and eliminates the need for an additional clamping circuit to give energy to the load. The performance analysis of the converter fed drive has also been carried out using MATLAB/Simulink and OPAL-RT SIL system to prove the viability of the converter in interfacing energy storage device to the dc link in electric vehicles. The converter successfully controls the power flow from the energy source to the motor and vice versa during forward motoring and regenerative braking.

In Section II, the topology and operation of the proposed HGBDC is covered, and in Section III, the specification and design of the converter fed drive system are discussed. The modelling and simulation of the converter fed drive in MATLAB/Simulink is given in Section IV. Section V describes the implementation of the proposed converter in RT-LAB real time simulation system. The summary of the work is presented in Section VI.

II. PROPOSED HIGH GAIN BIDIRECTIONAL DC-DC CONVERTER (HGBDC)

The proposed HGBDC shown in figure 1 has four active power switches (S_1, S_2, S_3, and S_4), two identical inductors (L_1 and L_2), a diode (D_1), and a capacitor (C_H) at the high voltage side. Diode D_1 helps in blocking the reverse voltage V_L appearing across the MOSFET while the switches S_1 and S_2 are conducting in boost mode. A switching frequency of f_s is used by the switches S_1, S_2, S_3, and S_4. During boost mode, switches S_1 and S_2 have a duty ratio of d_1, and switch

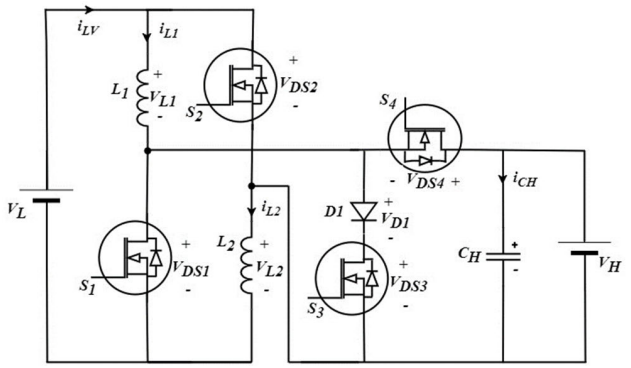

FIGURE 1. Proposed high gain bidirectional DC -DC converter (HGBDC).

S_3 has a duty ratio of d_2. The duty ratio of the switch S_4 is $(1\text{-}d_1\text{-}d_2)$ during boost mode and it is d_b during buck mode of operation of the converter.

A. OPERATION OF THE HGBDC IN BOOST MODE

The boost operation of the converter is explained in three different phases namely, Mode I, Mode II and Mode III. The current flow path of the proposed HGBDC operating in boost mode is depicted in figure 2. During this mode, the energy is transferred from the low voltage side to the high voltage side of the converter with the help of controlled switches S_1, S_2, S_3 and S_4. The switches S_1, S_2 and S_3 are operated through the PWM control. Typical waveforms of the proposed HGBDC in boost mode for continuous conduction are shown in figure 3.

1) MODE I

The switches S_1 and S_2 are turned on in this mode (t_0, t_1), while the switches S_3 and S_4 are turned off for the duration of d_1T_s. Energy flow is from the battery to the inductors L_1, L_2 which are connected in parallel, as shown in figure 2(a). The energy stored in the capacitor; C_H is released to the load. The voltage across the inductors is expressed in (1) to (3).

$$v_{L1} = v_{L2} = V_L \tag{1}$$

$$L_1\frac{di_{L1}}{dt} = L_2\frac{di_{L2}}{dt} = L\frac{di_L}{dt} = V_L \tag{2}$$

$$\frac{di_L}{dt} = \frac{V_L}{L} \tag{3}$$

where v_{L1} and v_{L2} are the voltages across inductors L_1 and L_2 respectively.

2) MODE II

Switch S_3 is active for the duration of d_2T_s, while switches S_1 and S_2 are turned off in Mode II (t_1, t_2). As displayed in figure 2(b), current flow is through L_1, D_1, S_3 and L_2. The energy from the source is delivered to the inductors. The load receives the energy that is stored in the capacitor. Source is in series with the inductors in this mode. Equations (4) and (5) represent the currents flowing through and the voltages across the inductors.

$$i_{L1} = i_{L2} \tag{4}$$

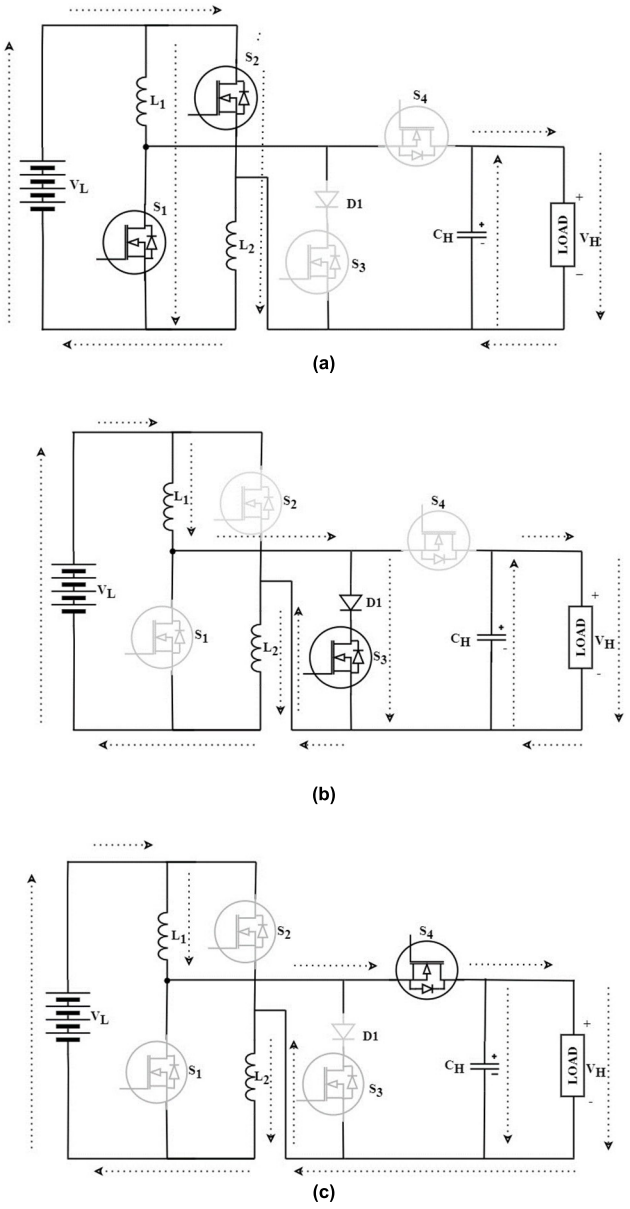

FIGURE 2. HGBDC in boost mode (a) Mode I (b) Mode II (c) Mode III.

where i_{L1} and i_{L2} are the current through inductors L_1 and L_2 respectively.

$$v_{L1} + v_{L2} = V_L \tag{5}$$

whereas,

$$v_{L1} = v_{L2} = L\frac{di_L}{dt} \tag{6}$$

$$\frac{di_L}{dt} = \frac{V_L}{2L} \tag{7}$$

3) MODE III

The MOSFET switches S_1, S_2 and S_3 are turned off in this mode (t_2, t_3), whereas the body diode of the MOSFET S_4 conducts during $(1\text{-}d_1\text{-}d_2)T_S$. Diode D_1 is reverse biased. The load is supplied by both the source and the inductors as depicted in figure 2(c). The capacitor C_H is in charging mode

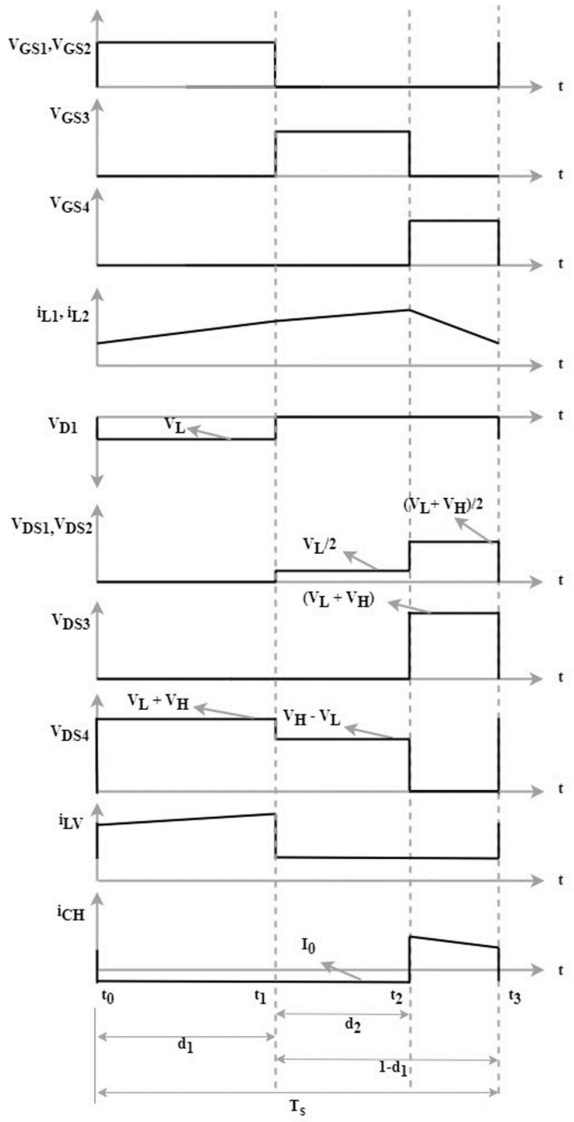

FIGURE 3. Operational waveforms of HGBDC in boost mode (CCM).

as the body diode of S_4 is forward biased. The inductors are connected in series to the source. The current through and the voltage across the inductors are given in (8) to (10).

$$i_{L1} = i_{L2} \tag{8}$$

$$v_{L1} + v_{L2} = V_L - V_H \tag{9}$$

$$v_{L1} = v_{L2} = L\frac{di_L}{dt} \tag{10}$$

From (9) and (10),

$$\frac{di_L}{dt} = \frac{V_L - V_H}{2L} \tag{11}$$

(3), (7), and (11) are combined to get (12) using the state space averaging technique:

$$\int_0^{d_1 T_s} \left(\frac{di_L}{dt}\right)^I dt + \int_0^{d_2 T_s} \left(\frac{di_L}{dt}\right)^{II} dt + \int_0^{(1-d_1-d_2)T_s} \left(\frac{di_L}{dt}\right)^{III} dt = 0 \tag{12}$$

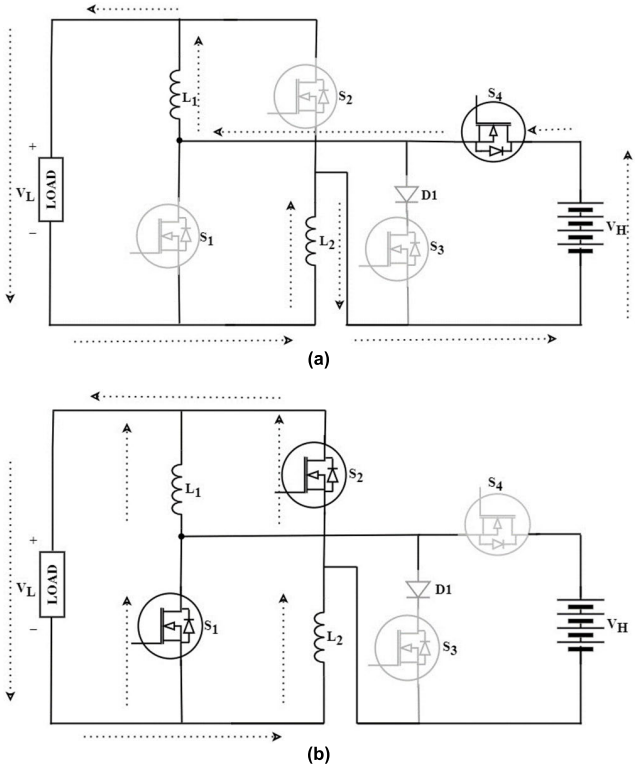

FIGURE 4. HGBDC in buck mode (a) Mode I (b) Mode II.

The modes of operation are indicated by the superscripts I, II, and III. The resulting voltage gain is given by (13).

$$\frac{V_H}{V_L} = \frac{(1+d_1)}{(1-d_1-d_2)} \tag{13}$$

B. OPERATION OF THE PROPOSED HGBDC IN BUCK MODE

The buck operation of the converter is explained in two different phases during the same switching cycle. The current flow path of the proposed HGBDC operating in buck mode is depicted in figure 4. Energy is transferred from the high voltage side to the low voltage side with the help of controlled switches S_4, S_1 and S_2 in this mode. The switch S_4 is operated through the PWM control with a duty ratio of d_b. Operational waveforms of the proposed HGBDC in buck mode for continuous conduction mode (CCM) are depicted in figure 5.

1) MODE I

In this mode (t_0, t_1), S_4 is turned on and $S_1/S_2/S_3$ are turned off for a duration of d_bT_s. The inductors L_1 and L_2, which are connected in series with the load and the battery, facilitate the transfer of energy from the high voltage side to the low voltage side of the converter as shown in figure 4(a). Equations (14) to (16) give the current flowing through and the voltage across the inductors in this mode.

$$i_{L1} = i_{L2} \tag{14}$$

$$v_{L1} + v_{L2} = V_H - V_L \tag{15}$$

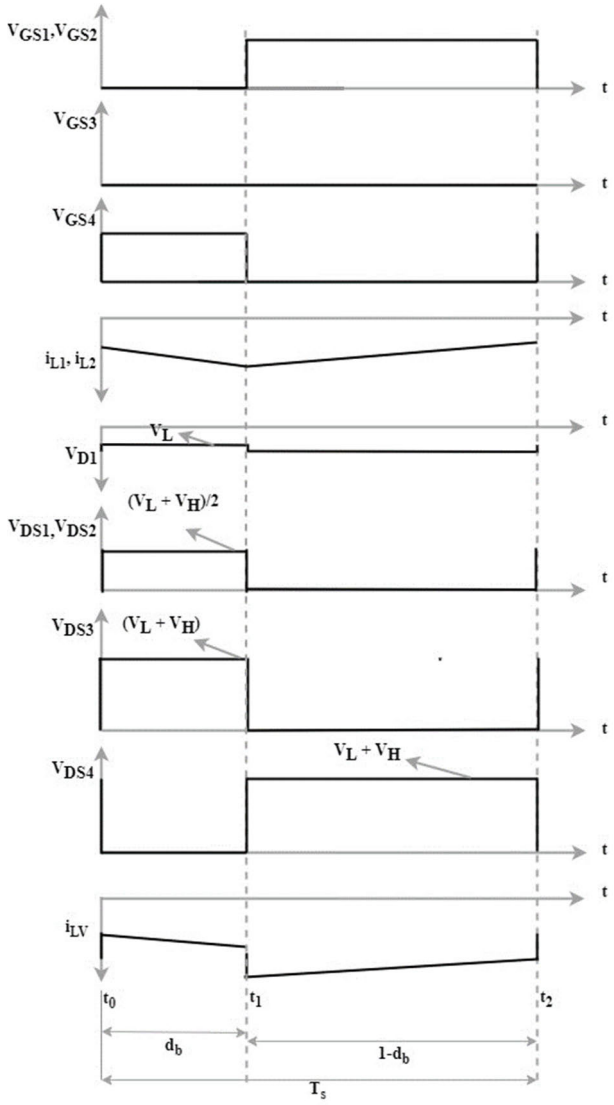

FIGURE 5. Operational waveforms of HGBDC in buck mode (CCM).

whereas,

$$v_{L1} = v_{L2} = L\frac{di_L}{dt}$$
$$\frac{di_L}{dt} = \frac{V_H - V_L}{2L} \tag{16}$$

2) MODE II

The body diodes of the MOSFETs S_1 and S_2 conduct for a duration of $(1-d_b)T_s$ in this mode (t_1, t_2), while the MOSFET S_4 is turned off. Figure 4(b) depicts the current flow path. Inductors L_1 and L_2 discharge their stored energy to the load on low voltage side. Because L_1 and L_2 are in parallel, the voltages across them are as given in (17).

$$v_{L1} = v_{L2} = -V_L \tag{17}$$
$$L\frac{di_{L1}}{dt} = L\frac{di_{L2}}{dt} = -V_L \tag{18}$$
$$\frac{di_L}{dt} = \frac{-V_L}{L} \tag{19}$$

Equations (16) and (19) are combined to get (20) using the state space averaging technique.

$$\int_0^{d_bT_s}\left(\frac{di_L}{dt}\right)^I dt + \int_0^{(1-d_b)}\left(\frac{di_L}{dt}\right)^{II} dt = 0 \tag{20}$$

The modes of operation are indicated by the superscripts I and II. The resulting voltage gain in buck mode is given by (21).

$$\frac{V_L}{V_H} = \frac{d_b}{(2-d_b)} \tag{21}$$

where, d_b is the duty ratio of the HGBDC in buck mode of operation.

C. EFFICIENCY ANALYSIS

In order to determine the theoretical efficiency curve and compute converter losses, the efficiency of the proposed converter is derived by taking the parasitic elements into consideration. To make the mathematical analysis simpler, the ripple in the capacitor voltage and inductor current is ignored. By taking these parasitic elements into consideration, the expression for voltage V_H at the high voltage side of the converter, is given by (22).

$$V_H = \frac{V_L(1+d_1) - V_{D1}d_2}{\left(\frac{2(d_1\alpha_1+d_2\alpha_2+(1-d_1-d_2)\alpha_3)}{R_H(1-d_1-d_2)}\right)+(1-d_1-d_2)} \tag{22}$$

where,

$$\begin{cases} \alpha_1 = r_{S1} + r_{L1} \\ \alpha_2 = \dfrac{(r_{S3} + r_{L1} + r_{L2} + r_{D1})}{2} \\ \alpha_3 = \dfrac{(r_{L1} + r_{L2} + r_{S4})}{2} \end{cases}$$

where, r_{L1} and r_{L2} are the ESR of the inductors L_1 and L_2 respectively. Similarly, r_{S1}, r_{S2}, r_{S3} and r_{S4} represent the ON-state resistances of the switches S_1, S_2, S_3 and S_4 respectively. r_{D1} and V_{D1} are the internal resistance and the voltage drop across the diode D_1 respectively. The resulting equation for efficiency of the proposed converter in boost mode of operation is given in (23).

$$\eta = \frac{P_H}{P_L} = \frac{\left(\frac{V_H^2}{R_H} - P_{SW}\right)}{\frac{V_L V_H(1+d_1)}{R_H(1-d_1-d_2)}} \tag{23}$$

where, P_H and P_L are the power at high voltage side and low voltage side of the converter respectively. R_H is the load resistance at high voltage side. P_{SW} is the switching loss across the power switches which is given by (24). The rise and fall time of the power switches are represented by t_r and t_f respectively.

$$P_{SW} = 0.5V_{DS}I_D\left(t_r + t_f\right)f_{SW} \tag{24}$$

The expression for voltage V_L at the low voltage side of the converter, by taking the parasitic elements into consideration

TABLE 1. Comparison of the proposed converter with other converters.

Bidirectional converter	Proposed converter	Other converter topologies in [12]	[16]	[17]	[19]	[21]	[24]	[25]
No. of inductors	2	3	2	2	2	-	-	-
No. of coupled inductors	0	-	-	-	-	1	1	1
No. of capacitors	1	6	6	6	4	3	2	6
No. of power switches/diodes	4/1	8	5	6/1	5	4	4	6
Voltage gain (boost)	$\frac{1+d_1}{1-d_1-d_2}$	$\frac{3}{1-d}$	$\frac{2+d}{1-d}$	$\frac{2}{1-2d}$	$\frac{2}{1-d}$	$\frac{1}{(1-d)^2}$	$\frac{n+1}{1-d}$	$\frac{2n+2}{1-d}$
Max. efficiency (boost)	95.7%	95.8%	94.09%	95.9%	95.21%	90%	94.5%	96.63%
Max. Efficiency (buck)	96.68%	95.9%	94.41%	94.8%	95.30%	91%	94%	96.12%
Frequency	50kHz	20kHz	20kHz	20kHz	20kHz	40kHz	50kHz	50kHz
Power level	3730W	1800W	400W	300W	1000W	250W	500W	250W
Applications	to interface a storage device to the dc link in EVs	to interface a storage device to the dc link in EVs	to interface a storage device to the dc link in EVs	to interface a storage device to the dc link in EVs	to interface storage element to dc bus	to interface a storage device to the dc link in EVs	to interface a storage device to the dc link	to interface a storage device to the dc link in EVs

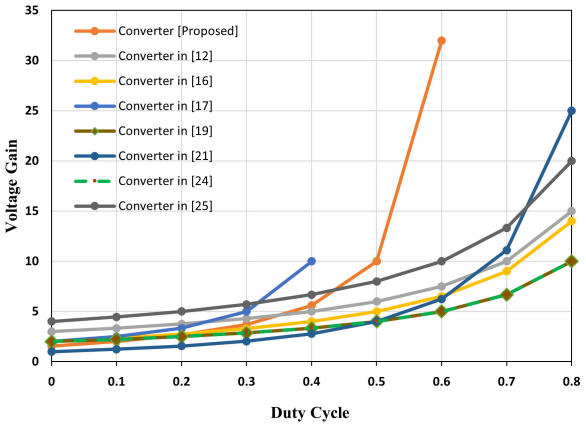

FIGURE 6. Voltage gain versus duty cycle of the converters.

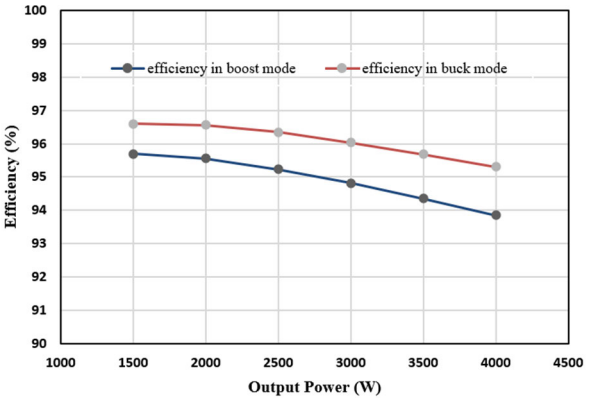

FIGURE 7. Efficiency versus output power of the proposed HGBDC.

is given in (25).

$$V_L = \left(\frac{d_b}{2-d_b}\right) \frac{(2-d_b)^2 R_L}{(2-d_b)^2 R_L + d_b\beta_1 + 2(1-d_b)\beta_2} \tag{25}$$

where,

$$\begin{cases} \beta_1 = r_{S4} + r_{L1} + r_{L2} \\ \beta_2 = r_{L1} + r_{S1} \end{cases}$$

The calculated efficiency of the proposed converter in step-down mode is given by (26).

$$\eta = \frac{P_L}{P_H} = \frac{\left(\frac{V_L^2}{R_L} - P_{SW}\right)}{\frac{d_b V_L V_H}{d_b(2-d_b)R_L}} \tag{26}$$

where, R_L is the load resistance at low voltage side.

D. COMPARISONS WITH OTHER CONVERTERS

A comparison of the proposed converter with similar non isolated bidirectional converters is listed in Table 1. The comparison is made in terms of voltage gain, number of inductors, capacitors and switches, frequency of operation, power level, intended application and efficiency. The proposed HGBDC uses only four power switches and one diode, which is minimal when compared to the converters in [12], [16], [17], [19], and [25]. The number of inductors and capacitors are also least in comparison with the other converters. In Figure 6, the voltage gain against duty cycle is plotted for each of these converters. The voltage gain of the proposed HGBDC is higher than in other converters between a duty cycle range of 0.45 to 0.6 as can be seen in figure 6. The proposed HGBDC uses two different duty ratios 'd_1' and 'd_2' to achieve high voltage gain. With a constant duty ratio 'd_2' as 0.35, 'd_1' is varied for plotting the graph. The converters in [24] and [25] use coupled inductors for which the turns ratio 'n' is taken as unity for plotting the graph. When duty ratio d_1 is at 0.6, the proposed HGBDC offers a high voltage gain of 32. However, the voltage gain of other converters are less than 15 for the same duty ratio.

TABLE 2. Parasitic parameters of components.

Parameter	Value	Parameter	Value
$r_{S1,2,3,4}$	11mΩ	V_{D1}	0.83V
$V_{f1,\,2,3,\,4}$	1.4V	r_{D1}	2.2mΩ
$t_{r1,2,3,4}$	30nS	r_{L1}	24mΩ
$t_{f1,2,3,4}$	14nS	r_{L2}	24mΩ

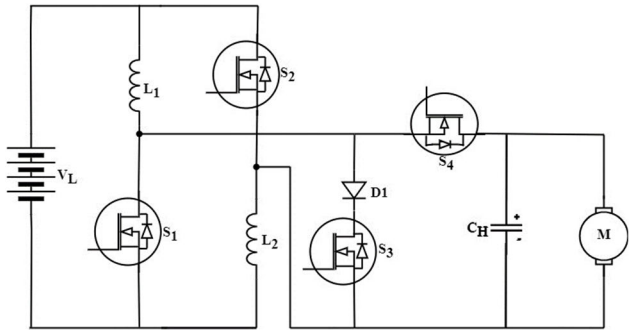

FIGURE 8. HGBDC connected to battery source and a dc motor load.

TABLE 3. Converter specifications.

Parameter	MATLAB/Simulink	RT-LAB
Input Voltage	48V	48V
Output Voltage	240V	240V
Switching Frequenc	50 kHz	5 kHz
Inductor L_1, L_2	200 µH	1000 µH
Capacitor C_H	300 µF	1000 µF
Load (DC motor)	5 HP, 240 V, 1750rpm	5 HP, 240 V, 1750 rpm

The efficiency of the proposed converter is calculated based on equations (23) and (26) for both boost and buck mode respectively. Table 2 lists the parasitic parameters of components for the MOSFET (IXFH120N30X3) and diode (STTH6004W) as given in the datasheets. ESR of the inductor is estimated to be 24 mΩ. The voltages at the high voltage side and low voltage side of the converter are 240V and 48V respectively. Theoretical efficiency curves in both boost and buck modes are plotted in figure 7. The calculated efficiency for a rated power of 3.73 kW is found to be 94.12% in boost mode and 95.51% in buck mode. The maximum efficiencies are 95.7% and 96.6% in boost and buck modes which are comparable to the efficiencies of the counterparts presented in Table 1 and better than that of the converter presented in [21]. Frequency, power level and intended application of the converters are also compared in Table 1. Even though the applications of the compared converters are meant for interfacing storage devices to the dc link, the performance analysis for the complete system is not discussed in the reference papers.

III. CONVERTER DESIGN AND MOTOR CONTROL

The proposed HGBDC may be used to test its viability for applications like electric automobiles by integrating it into a simple DC motor drive. In this work, the converter is operated in continuous conduction mode to drive the dc motor in forward motoring and regenerative braking modes. The HGBDC is connected to a battery and a dc motor load as shown in figure 8. The light electric vehicle industry makes extensive use of DC motors, which are chosen for their simplicity and to check the viability of the converter operation in the proposed scheme. A 5 HP separately excited DC motor model rated at 240 V and 1750 rpm is utilized as the load to analyze the performance of the HGBDC in both MATLAB/Simulink and the OP4500 real-time simulation mode. The converter specifications are given in Table 3. The simulation makes use of the lithium ion (Li-ion) battery, whose specifications are listed in Table 4. The lithium-ion battery has a strong possibility of replacing other batteries as the foreseeable future of electric vehicle batteries. This is due to its fascinating properties including large power density, high energy density, extended life cycle, absence of memory effect, and superior energy efficiency. During regenerative braking, the proposed BDC transfers power from the motor back to the battery, and when the vehicle is moving, it delivers power from the battery to the DC motor.

TABLE 4. Battery parameters.

Parameter	Value/Specifications
Type	Li-ion
Nominal Voltage	48 V
Initial %SoC	80
Battery Capacity	140 Ah
Nominal Discharge Current	60.87 A

A. INDUCTOR DESIGN

The selection of an inductor is influenced by the motoring mode of operation, which in turn depends on the input voltage (V_L), current ripple (Δ_{iL}), frequency of switching (f_s), and the duty cycle (d_1). The critical inductance value for the operation of the proposed HGBDC in CCM is determined using (27).

$$L_{1,critical} = L_{2,critical} = \frac{V_L d_1}{\Delta i_L f_s} \tag{27}$$

The inductor has been designed with 50 kHz switching frequency and a specified current ripple which is considered as 12% of the input current.

B. CAPACITOR DESIGN

The rated power (P_o) of the converter, load voltage (V_o), ripple voltage (ΔV_c), and the frequency of switching (f_s), are used to calculate the value of the capacitor, C_H on the high voltage side using (28).

$$C_{o,critical} = \frac{P_o}{V_o \Delta V_c f_s} \tag{28}$$

A voltage ripple of 1% of the output voltage, V_H is used for the design of the capacitor.

C. VOLTAGE STRESS OF THE SWITCH AND DIODE

The voltage stress V_{DS1}, V_{DS2}, V_{DS3} and V_{DS4} across switches S_1 and S_2, S_3 and S_4 for boost mode of operation

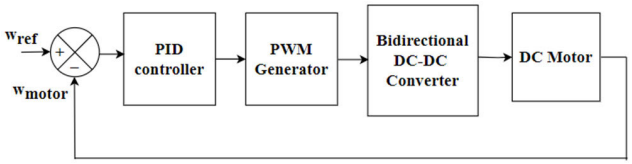

FIGURE 9. Block diagram of closed loop control scheme.

are given by (29), (30) and (31).

$$V_{DS1} = V_{DS2} = \frac{V_H + V_L}{2} \tag{29}$$

$$V_{DS3} = V_H \tag{30}$$

$$V_{DS4} = V_H + V_L \tag{31}$$

The voltage stress V_{D1} on the diode D_1 for both buck and boost mode of operations are given by equation (32).

$$V_{D1} = V_L + V_H \tag{32}$$

The voltage stress V_{DS1}, V_{DS2}, V_{DS3} and V_{DS4} across switches S_1 and S_2, S_3 and S_4 for buck operation are given in (33) and (34).

$$V_{DS1} = V_{DS2} = \frac{V_H + V_L}{2} \tag{33}$$

$$V_{DS3} = V_{DS4} = V_H + V_L \tag{34}$$

D. CONTROL TECHNIQUE

A practical technique for adjusting the speed of the drive is to control the output voltage of the BDC. A PID controller is used to ensure that the vehicle reaches the target speed and reacts quickly to rapid changes in speed without oscillations. Figure 9 depicts the control circuitry for the HGBDC. It senses the motor speed ω_{motor} and compares it to the reference speed ω_{ref}. The error signal is processed by the PID controller and compared to a high-frequency sawtooth signal to generate the PWM control signals.

IV. MODELLING AND SIMULATION

The HGBDC fed DC motor drive is modelled and simulated using MATLAB/Simulink for a duration of 10 seconds. The steady-state inductor current and the gate drive pulses of the MOSFET switches for both boost and buck mode of operations of the converter are shown in figure 10 and figure 11 respectively. In boost (forward motoring) mode, the inductor current increases when the first three switches S_1, S_2 and S_3 are turned on, whereas the current through the inductor decreases when the switch S_4 is turned on. As shown in figure 10, the average value of the inductor current in steady state is 32 A. During buck (regenerative braking) mode, the steady-state inductor current is -13.5A. Negative value of the inductor current shows the reversal of current flow from the load to source; hence the power flow. Battery is charged from the regenerative power during this braking mode. For a rated speed of 1750 rpm in forward motoring mode, the duty ratio of the PWM pulses generated by the PWM controller, d_1 and d_2 for the switches S_1/S_2 and S_3 respectively are 0.455 and

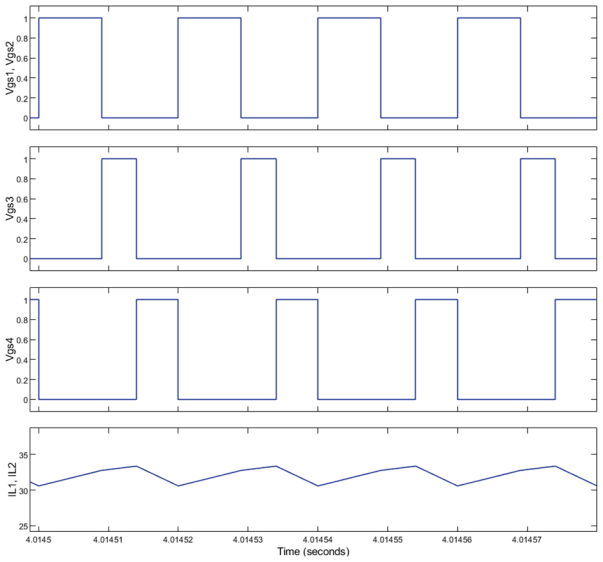

FIGURE 10. Switching signals for S_1, S_2, S_3, S_4 and inductor currents in boost mode of operation.

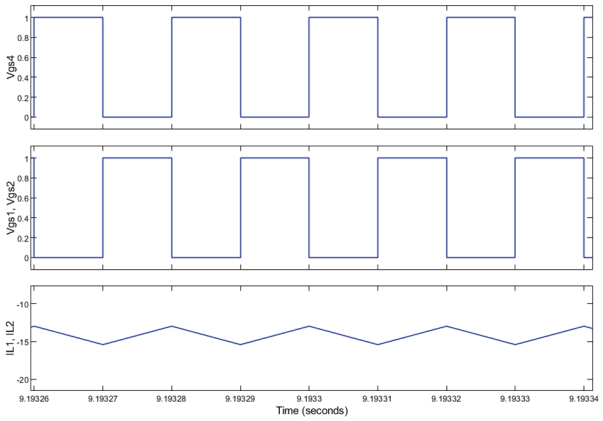

FIGURE 11. Switching signals for S_1, S_2, S_3, S_4 and inductor currents in boost mode of operation.

0.245 for a voltage gain of 4.85. During regenerative braking mode, the switch S_4 operates with a duty ratio d_b which is 0.5 and the corresponding voltage gain is 1/3 for a speed of 1150 rpm.

Two different cases are considered for analyzing the dynamics of the system:

(i) transition of the motor operation from forward motoring to regenerative braking.

(ii) a step change in speed during forward motoring.

A. TRANSITION OF THE MOTOR OPERATION FROM FORWARD MOTORING TO REGENERATIVE BRAKING

The converter is made to operate in boost (forward motoring) mode from 0-5 seconds and in buck (regenerative braking) mode from 5–10 seconds. Figure 12 shows the motor speed, armature torque, armature current, armature voltage (output voltage V_H) of the converter, battery SoC and battery voltage for this case. Simulations are carried out for the braking

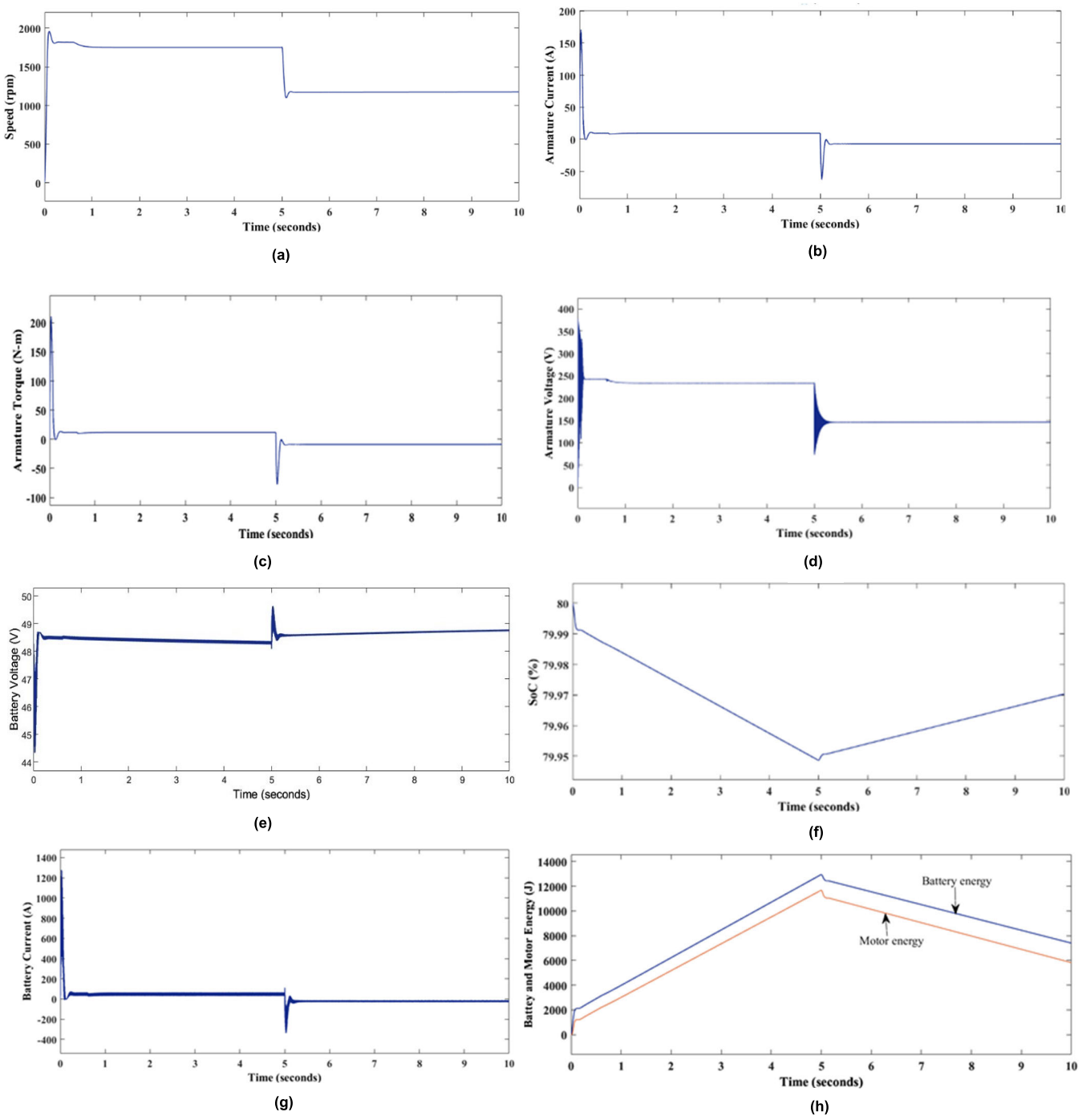

FIGURE 12. Simulation results for case1- transition of the motor from forward motoring to regenerative braking: (a) speed, (b) armature current, (c) armature torque, (d) armature (output) voltage of the motor, (e) battery voltage and (f) battery SoC (g) battery current (h) battery and motor energy.

action with a speed change from 1750 rpm to 1150 rpm when the motor current and torque exhibit a reversal characteristic as shown in figure 12(a), 12(b) and 12(c) respectively. The change in directions of current and torque during the transition from motoring mode to regenerative braking mode indicates the reversal of power flow. As seen in figure 12(d) armature voltage decreases in proportion to the decrease in speed. There is a dip in battery voltage and reduction in SOC of the battery during forward motoring (0 to 5 seconds). But the battery voltage and SoC of the battery increases during regenerative braking as observed in figure 12(e) and 12(f). The SoC of the battery increases by 0.02% from 79.95 to 79.97 during a short span of 5s in regenerative braking mode. The battery current and the energies of battery and motor are

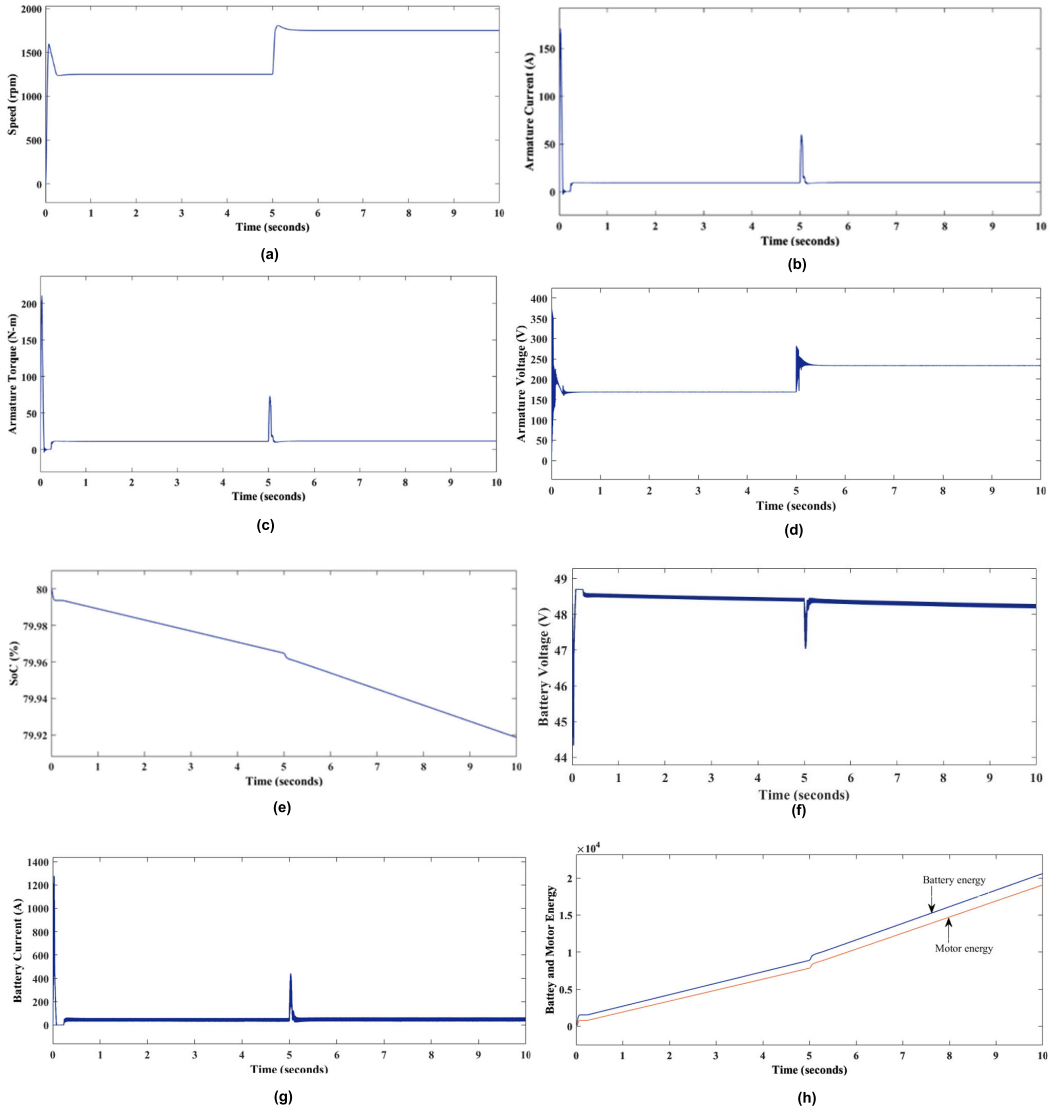

FIGURE 13. Simulation results for case 2- step change in speed during forward motoring: (a) speed, (b) armature current, (c) armature torque, (d) armature voltage, (e) battery SoC, (f) battery voltage, (g) battery current and (h) battery and motor energy.

shown in figure 12(g) and 12(h) respectively. Around 5000J of energy is recovered during regenerative braking.

B. A STEP CHANGE IN SPEED DURING FORWARD MOTORING

A step change in motor speed from 1250 RPM to 1750 RPM at constant torque constitutes the second instance of transient operation. Figure 13(a) depicts the speed waveform for a duration of 10 seconds. It is observed that the system settles down at the new speed within 0.5 seconds. The momentary change in armature torque caused by a sudden alteration in the speed is seen in Figure 13(c). The characteristics of current that is identical to that of torque is shown in figure 13(b). The change in armature voltage with respect to the change in motor speed is depicted in figure 13(d). As seen in figure 13(e), when the speed increases, the motor draws more energy from the source, resulting in a fall in the SoC of

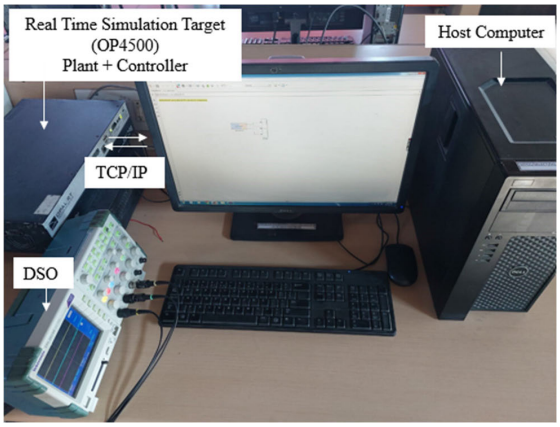

FIGURE 14. Real-time software in loop test platform.

the battery by 0.08%. The battery voltage and current during this phase are depicted in figures 13(f) and 13(g) respectively.

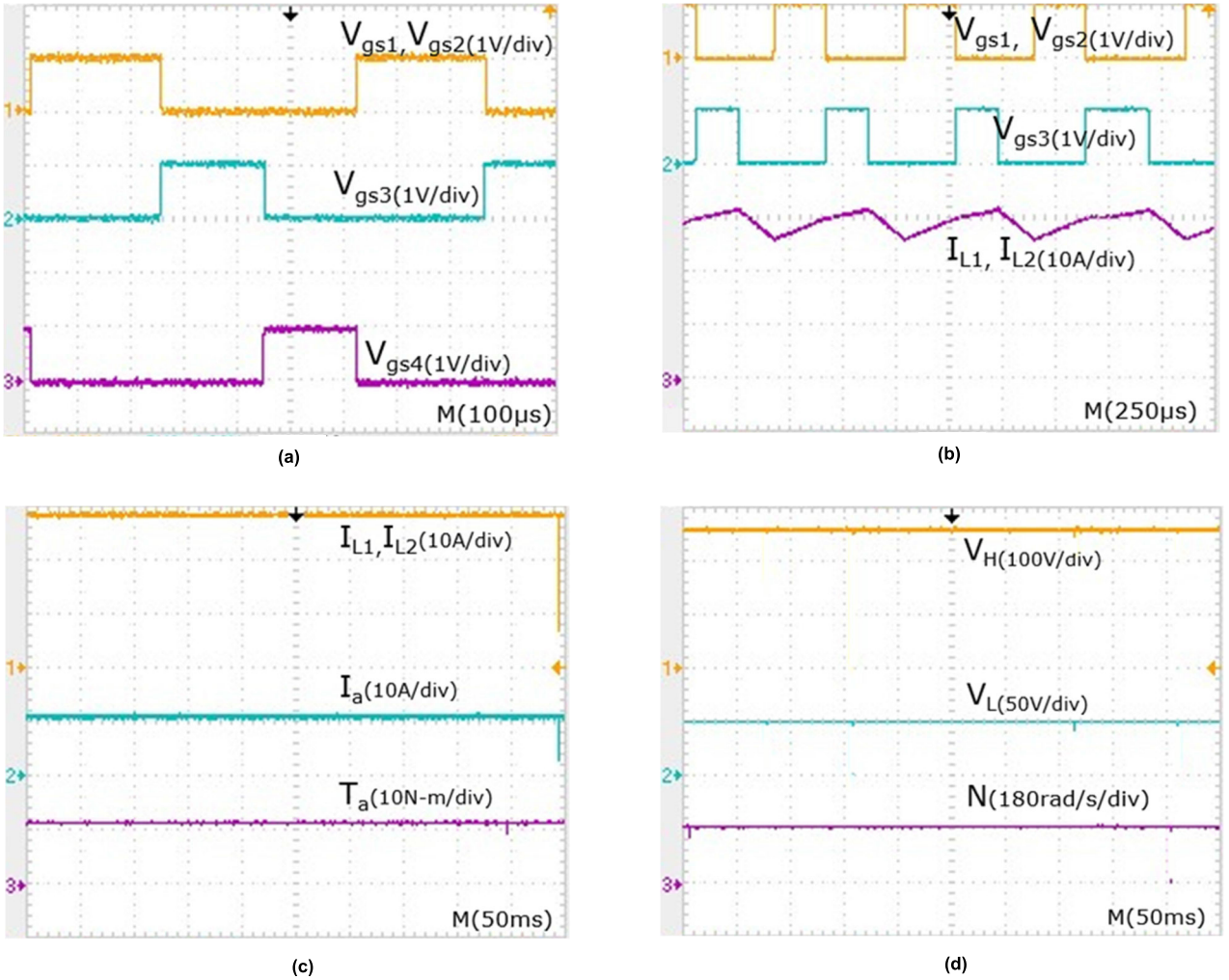

FIGURE 15. Real time simulation results (RT-LAB) of the HGBDC during motoring mode: (a) gate pulses V_{gs1} & V_{gs2} (CH1), V_{gs3} (CH2) and V_{gs4} (CH3) (b). gate pulses V_{gs1} & V_{gs2} (CH1), V_{gs3} (CH2) and inductor currents I_{L1} & I_{L2} (CH3) (c). Inductor currents I_{L1} & I_{L2} (CH1), armature current I_a (CH2) and armature Torque T_a (CH3), (d) armature Voltage V_H (CH1), battery Voltage V_L (CH2) and speed N in rad/s (CH3).

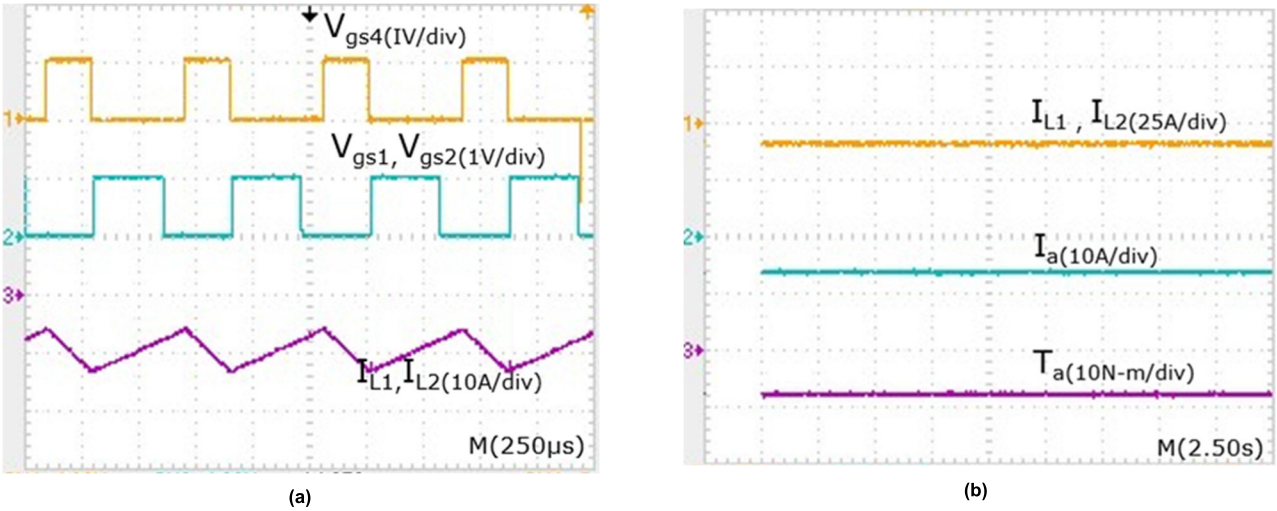

FIGURE 16. Real time simulation results (RT-LAB) of the HGBDC during regenerative braking: (a) gate pulses V_{gs4} (CH1), V_{gs1} & V_{gs2} (CH2), inductor currents I_{L1} & I_{L2} (CH3), (b) inductor currents I_{L1} & I_{L2} (CH1), armature current Ia (CH2) and armature torque T_a (CH3).

The battery and motor energy characteristics are shown in figure 13(h).

The theoretical efficiency of the of the proposed HGBDC is calculated for rated power and resistive load and is found

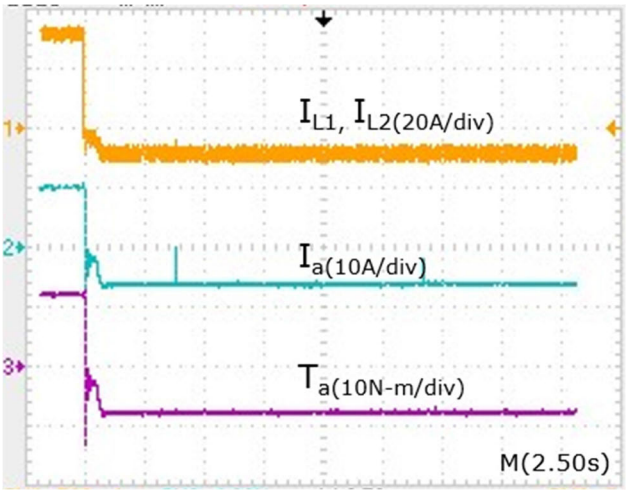

FIGURE 17. Switching of the motor from motoring mode to regenerative braking mode: inductor currents I_{L1} & I_{L2} (CH1), armature current I_a (CH2) and armature torque T_a (CH3).

to be 94.12% in boost mode and 95.51% in buck mode as discussed in section II-D. The results are in good agreement with the simulation results which are 94.57% and 95.05% respectively.

V. IMPLEMENTATION OF THE PROPOSED CONVERTER IN REAL-TIME SIMULATION SYSTEM

Software-in-the-loop (SIL) analysis is performed prior to real time Rapid Control Prototyping (RCP) or Hardware-in-the-Loop (HIL) testing of any system. The key advantage of SIL is that it does not require external input or output, ensuring signal consistency. Synchronization with the outside environment is hardly essential since the controller and the plant are functioning in the same simulator. In this section, both the controller and the plant are tested using a real-time simulator (OP4500) built on the RT-Lab platform.

The Simulink models of the battery, converter, motor, and associated control circuit are integrated with RT-Lab blocks and are accessible on the host computer which is linked to the OP4500 simulation target through a Transmission Control Protocol (TCP)/Internet Protocol (IP) communication network, as shown in figure 14. The OP4500 simulation target performs real-time computations for model inputs and outputs. To analyze the dynamics of the system, a step change in torque is applied and the forward motoring and regenerative braking modes are realized. Also, the impact of variation in speed during forward motoring mode is analyzed. The converter operating frequency is limited to 5 kHz to make it compatible with the existing RT-LAB platform.

Waveforms of the HGBDC operating in forward motoring (boost) mode are shown in figure 15. Gate pulses V_{gs1}, V_{gs2}, V_{gs3} and V_{gs4} are given in figure 15(a), whereas the steady-state inductor currents are displayed in figure 15(b), together with switching PWMs. The inductor currents I_{L1} and I_{L2}, armature current I_a, and armature torque T_a are positive during motoring (boost) mode and are shown in figure 15(c). Waveforms of the output voltage, input voltage and steady state speed are shown in figure 15(d). The waveforms for the buck mode of operation of the proposed HGBDC are shown in figure 16. The steady-state inductor currents I_{L1}, I_{L2}, and switching PWMs are shown in Figure 16(a). Figure 16(b) displays the waveforms for the inductor currents I_{L1} and I_{L2}, the armature current I_a, and the armature torque T_a. This demonstrates that the converter is operating in buck mode and that energy is successfully transferred from the DC motor to the battery.

The switching of the HGBDC fed drive from motoring mode to the regenerative braking mode is depicted in figure 17. The operation of the regenerative braking mode is indicated by negative torque and currents. It is observed that the results obtained using OPAL- RT software in loop test plat form is in good agreement with the simulation results obtained using MATLAB/Simulink.

VI. CONCLUSION

This paper focused on the design and development of a High Gain Bidirectional Converter (HGBDC) for electric vehicle applications with battery charging capability during regenerative braking. The performance analysis of the converter is carried out during motoring and regenerative braking modes in both MATLAB/Simulink and real time simulation environment with RT-LAB. The proposed method is simpler and the converter can attain high gain with the help of two duty cycle operation. It demonstrates a good balance among the voltage gain and the component counts which gives a viable solution to the application of interfacing storage devices to the DC link in electric vehicles which is the focus of the paper. The HGBDC also successfully controls the power flow direction by modifying the converter's working mode from motoring to regenerative braking. The efficiency of the proposed converter can further be improved by selecting SiC based power switches. Further Soft switching can be implemented to reduce the switching losses when the converter operates at higher frequency, but it adds complexity and increases the number of components.

REFERENCES

[1] C. H. T. Lee, W. Hua, T. Long, C. Jiang, and L. V. Iyer, "A critical review of emerging technologies for electric and hybrid vehicles," *IEEE Open J. Veh. Technol.*, vol. 2, pp. 471–485, 2021, doi: 10.1109/OJVT.2021.3138894.

[2] V. Rathore, K. Rajashekara, P. Nayak, and A. Ray, "A high-gain multilevel DC–DC converter for interfacing electric vehicle battery and inverter," *IEEE Trans. Ind. Appl.*, vol. 58, no. 5, pp. 6506–6518, Sep. 2022, doi: 10.1109/TIA.2022.3185183.

[3] H. Chen, H. Kim, R. Erickson, and D. Maksimovic, "Electrified automotive powertrain architecture using composite DC–DC converters," *IEEE Trans. Power Electron.*, vol. 32, no. 1, pp. 98–116, Jan. 2017, doi: 10.1109/TPEL.2016.2533347.

[4] A. Gupta, R. Ayyanar, and S. Chakraborty, "Novel electric vehicle traction architecture with 48 V battery and multi-input, high conversion ratio converter for high and variable DC-link voltage," *IEEE Open J. Veh. Technol.*, vol. 2, pp. 448–470, 2021, doi: 10.1109/OJVT.2021.3132281.

[5] J. O. Estima and A. J. M. Cardoso, "Efficiency analysis of drive train topologies applied to electric/hybrid vehicles," *IEEE Trans. Veh. Technol.*, vol. 61, no. 3, pp. 1021–1031, Mar. 2012, doi: 10.1109/TVT.2012.2186993.

[6] D. Sha, D. Chen, and J. Zhang, "A bidirectional three-level DC–DC converter with reduced circulating loss and fully ZVS achievement for battery charging/discharging," *IEEE J. Emerg. Sel. Topics Power Electron.*, vol. 6, no. 2, pp. 993–1003, Jun. 2018, doi: 10.1109/JESTPE.2017.2778039.

[7] T. Zhu, F. Zhuo, F. Zhao, F. Wang, H. Yi, and T. Zhao, "Optimization of extended phase-shift control for full-bridge CLLC resonant converter with improved light-load efficiency," *IEEE Trans. Power Electron.*, vol. 35, no. 10, pp. 11129–11142, Oct. 2020, doi: 10.1109/TPEL.2020.2978419.

[8] Y. Shen, H. Wang, A. Al-Durra, Z. Qin, and F. Blaabjerg, "A bidirectional resonant DC–DC converter suitable for wide voltage gain range," *IEEE Trans. Power Electron.*, vol. 33, no. 4, pp. 2957–2975, Apr. 2018, doi: 10.1109/TPEL.2017.2710162.

[9] C. Bai, B. Han, B.-H. Kwon, and M. Kim, "Highly efficient bidirectional series-resonant DC/DC converter over wide range of battery voltages," *IEEE Trans. Power Electron.*, vol. 35, no. 4, pp. 3636–3650, Apr. 2020, doi: 10.1109/TPEL.2019.2933408.

[10] N. Hou and Y. W. Li, "Overview and comparison of modulation and control strategies for a nonresonant single-phase dual-active-bridge DC–DC converter," *IEEE Trans. Power Electron.*, vol. 35, no. 3, pp. 3148–3172, Mar. 2020, doi: 10.1109/TPEL.2019.2927930.

[11] F. Zahin, A. Abasian, and S. A. Khajehoddin, "An alternative dual active bridge modulation to minimize RMS current and extend ZVS range," in *Proc. IEEE Energy Convers. Congr. Exposit. (ECCE)*, Detroit, MI, USA, Oct. 2020, pp. 5952–5959, doi: 10.1109/ECCE44975.2020.9235374.

[12] Y. Zhang, W. Zhang, F. Gao, S. Gao, and D. J. Rogers, "A switched-capacitor interleaved bidirectional converter with wide voltage-gain range for super capacitors in EVs," *IEEE Trans. Power Electron.*, vol. 35, no. 2, pp. 1536–1547, Feb. 2020, doi: 10.1109/TPEL.2019.2921585.

[13] Y. Zhang, Y. Gao, L. Zhou, and M. Sumner, "A switched-capacitor bidirectional DC–DC converter with wide voltage gain range for electric vehicles with hybrid energy sources," *IEEE Trans. Power Electron.*, vol. 33, no. 11, pp. 9459–9469, Nov. 2018, doi: 10.1109/TPEL.2017.2788436.

[14] S. T. S. Lee, S. Y. R. Hui, W. C. Chow, and H. S. H. Chung, "Development of a switched-capacitor DC–DC converter with bidirectional power flow," *IEEE Trans. Circuits Syst. I, Fundam. Theory Appl.*, vol. 47, no. 9, pp. 1383–1389, Sep. 2000, doi: 10.1109/81.883334.

[15] D. F. Cortez, G. Waltrich, J. Traigneaud, H. Miranda, and I. Barbi, "DC–DC converter for dual-voltage automotive systems based on bidirectional hybrid switched-capacitor architectures," *IEEE Trans. Ind. Electron.*, vol. 62, no. 5, pp. 3296–3304, May 2015, doi: 10.1109/TIE.2014.2350454.

[16] Y. Zhang, Q. Liu, Y. Gao, J. Li, and M. Sumner, "Hybrid switched-capacitor/switched-quasi-Z-source bidirectional DC–DC converter with a wide voltage gain range for hybrid energy sources EVs," *IEEE Trans. Ind. Electron.*, vol. 66, no. 4, pp. 2680–2690, Apr. 2019, doi: 10.1109/TIE.2018.2850020.

[17] A. Kumar, X. Xiong, X. Pan, M. Reza, A. R. Beig, and K. A. Jaafari, "A wide voltage gain bidirectional DC–DC converter based on quasi Z-source and switched capacitor network," *IEEE Trans. Circuits Syst. II, Exp. Briefs*, vol. 68, no. 4, pp. 1353–1357, Apr. 2021, doi: 10.1109/TCSII.2020.3033048.

[18] Z. Wang, P. Wang, B. Li, X. Ma, and P. Wang, "A bidirectional DC–DC converter with high voltage conversion ratio and zero ripple current for battery energy storage system," *IEEE Trans. Power Electron.*, vol. 36, no. 7, pp. 8012–8027, Jul. 2021, doi: 10.1109/TPEL.2020.3048043.

[19] Y. Zhang, Y. Gao, J. Li, and M. Sumner, "Interleaved switched-capacitor bidirectional DC–DC converter with wide voltage-gain range for energy storage systems," *IEEE Trans. Power Electron.*, vol. 33, no. 5, pp. 3852–3869, May 2018, doi: 10.1109/TPEL.2017.2719402.

[20] L.-S. Yang and T.-J. Liang, "Analysis and implementation of a novel bidirectional DC–DC converter," *IEEE Trans. Ind. Electron.*, vol. 59, no. 1, pp. 422–434, Jan. 2012, doi: 10.1109/TIE.2011.2134060.

[21] A. R. N. Akhormeh, K. Abbaszadeh, M. Moradzadeh, and A. Shahirinia, "High-gain bidirectional quadratic DC–DC converter based on coupled inductor with current ripple reduction capability," *IEEE Trans. Ind. Electron.*, vol. 68, no. 9, pp. 7826–7837, Sep. 2021, doi: 10.1109/TIE.2020.3013551.

[22] B. Li, P. Wang, Z. Wang, X. Ma, and H. Bi, "A new coupled-inductor-based high-gain interleaved DC–DC converter with sustained soft switching," *IEEE Trans. Veh. Technol.*, vol. 70, no. 7, pp. 6527–6541, Jul. 2021, doi: 10.1109/TVT.2021.3083317.

[23] Y. Zhang, H. Liu, J. Li, and M. Sumner, "A low-current ripple and wide voltage-gain range bidirectional DC–DC converter with coupled inductor," *IEEE Trans. Power Electron.*, vol. 35, no. 2, pp. 1525–1535, Feb. 2020, doi: 10.1109/TPEL.2019.2921570.

[24] M. Das and V. Agarwal, "Design and development of a novel high voltage gain, high-efficiency bidirectional DC–DC converter for storage interface," *IEEE Trans. Ind. Electron.*, vol. 66, no. 6, pp. 4490–4501, Jun. 2019, doi: 10.1109/TIE.2018.2860539.

[25] S. B. Santra, D. Chatterjee, and T.-J. Liang, "High gain and high-efficiency bidirectional DC–DC converter with current sharing characteristics using coupled inductor," *IEEE Trans. Power Electron.*, vol. 36, no. 11, pp. 12819–12833, Nov. 2021, doi: 10.1109/TPEL.2021.3077584.

[26] M. Lakshmi and S. Hemamalini, "Nonisolated high gain DC–DC converter for DC microgrids," *IEEE Trans. Ind. Electron.*, vol. 65, no. 2, pp. 1205–1212, Feb. 2018, doi: 10.1109/TIE.2017.2733463.

C. P. RAGASUDHA received the B.Tech. degree in electrical and electronics engineering from the Government College of Engineering Kannur, Kerala, India, in 2002, and the M.Tech. degree in computer applications in industrial drives from the M. S. Ramaiah Institute of Technology (affiliated to VTU Belgaum), Bengaluru, India, in 2012. She is currently pursuing the Ph.D. degree in design and analysis of power converters for electric vehicle applications with the School of Electrical Engineering, VIT University, Chennai. Her research interests include power electronics applications in electric vehicles and renewable energy, high gain dc–dc converters, and multiport converters. She is a Lifetime Member of the Indian Society for Technical Education.

S. HEMAMALINI (Senior Member, IEEE) received the Ph.D. degree in power systems from the National Institute of Technology, Tiruchirappalli, India, in 2011. She is currently a Professor with the School of Electrical Engineering, Vellore Institute of Technology, Chennai Campus, Chennai, India. She has about 28 years of teaching and research experience. Her current research interests include power system optimization, renewable energy, microgrids, power electronics applications in power systems, reliability, artificial intelligence—machine learning applications, protection in microgrids, and electric vehicles. She is a Lifetime Member of the Indian Society for Technical Education.